E. A. Ayrjan, V. D. Grouba*, S. N. Sidorenko*

THE ROLE OF THE ION–MOLECULE AND MOLECULE–MOLECULE INTERACTIONS IN THE FORMATION OF THE TWO-ION AVERAGE FORCE INTERACTION POTENTIAL

*Computation Physics Laboratory, Russian Peoples' Friendship University, Moscow, Russia

INTRODUCTION

The effect of solvent on electrolyte properties has already been a central problem in physical chemistry for several decades. The need for taking into account this effect arises both in describing the ion solvation under infinite dilution and in calculating thermodynamic properties of real solutions [2]. The continual [3,4] and semi-phenomenological quasi-discrete [2,5] approaches are no longer effective because the new qualitative concepts have to be developed regarding the liquid phase structure (i. e. the structures of the solvent per se and the ion pairs together with their salvation shell). Such notions as "solvent structure", "effect of ions on solvent structure", "effect of solvent structure on ion association", etc. are extensively used often without sufficient ground and also without assigning any specific physical meaning. This situation may be remedied by using discrete solvent models and giving equal regard to all its constituent particles (molecules and ions). This work deals with the chief aspects of the formation of mean force potential (MFP) of ion-molecule and molecule–molecule interact $\omega_{ab}(r)$. Thereby we hope to gain an insight into the relationship between the form of the short-range ion distribution function and the solvent properties, especially its structure, since the latter is influenced by the molecule–molecule interactions.

We shall use the results of [6] and consider spherical ions (suffixes "a" and "b") at infinite dilution and spherical solvent molecules (suffix "s") having a central dipole moment P_s. According to [6],

$$-\frac{1}{RT}\omega_{ab}(R) = -\frac{1}{RT}\varphi_{ab}(R) + g_{ab}(R) + \sum_{n\geq 1} F_{ab}^{(n+2)}(R) \qquad (1)$$

where k is the Boltzmann constant; T is temperature, K; R is the distance between ions; $\varphi_{ab}(R)$ is direct (pairwise) short–range potential; $g_{ab}(R)$ is the screened potential; $F_{ab}^{(n+2)}(R)$ is the $(n+2)$ -th virial coefficient.

Under infinite dilution, the screened potential g_{ab} has a simple form:

$$g_{ab}(R) = -\frac{e^2 Z_a Z_b}{\varepsilon_0 kT R} \qquad (2)$$

where e is the electron charge; Z_a, Z_b are the ion valences; ε_0 is the self-consistent part of the solvent permittivity:

$$\varepsilon_0 = 1 + \frac{4}{3}\pi \frac{N_s}{V}\frac{P_s^2}{kT}, \qquad (3)$$

where N_s is the number of solvent molecules in a volume V.

A study of the binary functions of particle distribution in mixtures has shown [7] that the theory proposed in [6] leads to physically authentic results throughout the ion concentration range.

Below we consider the approximations of the third and fourth virial coefficients and the effect of the elementary diagram of the fourth virial coefficient. We shall thus be able to see what should happen if the solvent "structure" is not (third virial coefficient) or is (the other approximations) taken into account. We shall also consider the effect of density and the dipole moment of the solvent molecules on $\omega_{ab}(R)$. Our computer could not determine the higher order terms of the virial series (1), nonetheless our results adequately describe all basic properties of real solutions.

CALCULATION FORMULAS

The calculation formulas are:

$$F_{ab}^{(3)} = \frac{2\pi}{r} n_s^* \int\limits_0^\infty s\,ds \int\limits_{|r-s|}^{r+s} t\,dt \Psi_{ab}(s,t);$$

$$\Psi_{ab}(s,t) = \exp\{-\frac{1}{RT}(\varphi_{as}(s) + \varphi_{bs}(t))\}\frac{\sin hG_{ab}(s,t)}{G_{ab}(s,t)} -$$

$$- \exp\{-\frac{1}{RT}\varphi_{as}(s)\}\frac{\sin hG_a(s)}{G_a(s)} - \exp\{-\frac{1}{RT}\varphi_{sb}(t)\}+ \qquad (4)$$

$$+1 - \frac{1}{3}G_a(s)G_b(t);$$

$$G_{ab}(s,t) = G_a(s) + G_b(t);$$

$$G_a(s) = \begin{cases} q_{as}\dfrac{1}{s^2}; & s \geqslant 1; \\ 0; & s < 1; \end{cases}$$

$$q_{as} = \frac{ez_a P_s}{RT\sigma_{+-}^2 \varepsilon_0};$$

$$F_{ab}^{(4)}(R) = \text{[diagram]} + \text{[diagram]} + \text{[diagram]} + \frac{1}{2}s\,\text{[diagram]}$$

2

$$\circ\!\!-\!\!\!-\!\!\!-\!\!\!-\!\!\!-\!\!\circ = \Psi_{as}(R,\Omega_s) \qquad or \qquad \Psi_{ss}(R,\Omega_1,\Omega_2);$$

$$\circ\!\!-\!\!\!-\!\!\!-\!\!\!-\!\!\circ = g_{as}(R,\Omega_s) \qquad or \qquad g_{ss}(R,\Omega_1,\Omega_2);$$

$$\circ\!\!-\!\!-\!\!-\!\!-\!\!\circ = F_{as}^{(3)}(R,\Omega_s)(\Psi_{as}(R,\Omega_s)+1);$$

$$\circ\!\!\sim\!\!\sim\!\!\sim\!\!\circ = \bigwedge$$

$$\circ\!\!-\!\!-\!\!-\!\!-\!\!\circ = F_{as}^{(3)}(R,\Omega_s)\Psi_{as}(R) - \circ\!\!\sim\!\!\sim\!\!\sim\!\!\circ$$

$$\Psi_{as}(R,\Omega_s) = \exp\{g_{as}(R,\Omega_s) - \frac{1}{RT}\varphi_{as}(R)\} - 1;$$

$$\Psi_{ss}(R,\Omega_1,\Omega_2) = \exp\{g_{ss}(R_1,\Omega_1,\Omega_2) - \frac{1}{RT}\varphi_{ss}(R)\} - 1;$$

$$g_{as} = (R,\Omega_s) = G_a(R)\cos\vartheta_s; \tag{5}$$

$$g_{ss}(R,\Omega_1,\Omega_2) = G_s(R)(2\cos\vartheta_1\cos\vartheta_2 - \sin\vartheta_1\sin\vartheta_1\cos(\varphi_1-\varphi_2));$$

$$G_s(t) = \begin{cases} W_{ss}\dfrac{1}{t^3}, & t \geqslant 1; \\ 0, & t < 1; \end{cases}$$

$$W_{ss} = \frac{P_s^2}{RT\sigma_{+-}^3\varepsilon_0}$$

$$r = R/\sigma_{+-}; \qquad \sigma_{+-} = r_0^+ + r^-;$$

P_s is the dipole moment, e is the electron charge, and are the valences of ions of the ath and B^{th} sorts, $\varphi_{ab}, \varphi_{as}, \varphi_{ss}$ are the pairwise shortrange potentials of the ion-ion, ion-molecule and molecule-molecule interactions correspondingly, $\Omega_1 = (\vartheta_s,\varphi_s)$ are the polar angles of the Sth molecule, $d\Omega_s = \frac{1}{4\pi}\sin\vartheta_s d\vartheta_s d\varphi_s$.

Integrating over orientations and using the bipolar coordinate system we obtain

$$F_{ab}^{*(3)} = \frac{2\pi}{r}n_s^* \int\limits_0^\infty sds \int\limits_{|r-s|}^{r+s} tdt\Psi_{as}^*(s,t,\vartheta_s); \tag{6}$$

$$\Psi_{as}^*(s,t,\vartheta_s) = \exp[-\frac{1}{RT}(\varphi_{as}(s)+\varphi_{ss}(t))]\frac{\sin hG_{as}(s,t)}{G_{as}(s,t)} -$$

$$- \exp[-\frac{1}{RT}\varphi_{as}(s)]\frac{\sin hG_a(s)}{G_a(s)} -$$

$$- \exp[-\frac{1}{RT}\varphi_{ss}(t)]\frac{\sin h(G_s(t))\sqrt{1+3\cos^2\vartheta_s}}{G_s(t)\sqrt{1+3\cos^2\vartheta_s}} - \frac{2}{3}G_a(s)G_s(t)\cos\vartheta_s;$$

$$G_{as}(s,t) = \sqrt{G_a^2(s) + G_s^2(t)(1+3\cos^2\vartheta_s) - 4G_a(s)G_s(t)\cos\vartheta_s}.$$

$$\frac{1}{2}\;\boxtimes\; = \frac{\pi}{r^2}(n_s^*)^2 \int\limits_0^\infty s\,ds \int\limits_{|s-r|}^{s+r} t\,dt \int\limits_0^\infty u\,du \times$$

$$\times \int\limits_{|u-r|}^{u+r} v\,dv \int\limits_0^\pi d\varphi \int\limits_{-1}^{+1} dx E(s,t,u,v,z,x),$$

$$z^2 = (s^2 + u^2) - \frac{1}{2r^2}(r^2+s^2-t^2)(u^2+r^2-v^2)+$$

$$+ \frac{1}{2r^2}[4r^2s^2 - (r^2+s^2-t^2)^2]^{1/2} \times$$

$$\times [4r^2u^2 - (r^2+u^2-v^2)^2]^{1/2}\cos\varphi,$$

$$E(s,t,u,v,z,x) = F(s)F(t)F(u)F(v)F(z)\times$$

$$\times \exp[x\left(\frac{q_a}{s^2} + \frac{q_b}{t^2}\right)]\frac{\sin hL_{ab}}{L_{ab}} -$$

$$-F(s)F(t)F(u)F(v)\exp[x\left(\frac{q_a}{s^2} + \frac{q_b}{t^2}\right)]\frac{\sin hG_{ab}^{(1)}}{G_{ab}^{(1)}} -$$

$$-F(s)F(t)F(v)F(z)\exp[x\left(\frac{q_a}{s^2} + \frac{q_b}{t^2}\right)]\frac{\sin hG_{ab}^{(2)}}{G_{ab}^{(2)}} -$$

$$-F(s)F(t)F(u)F(z)\exp[x\left(\frac{q_a}{s^2} + \frac{q_b}{t^2}\right)]\frac{\sin hG_{ab}^{(3)}}{G_{ab}^{(3)}} -$$

$$-F(s)F(u)F(v)F(z)\exp\left(x\frac{q_a}{s^2}\right)\frac{\sin hL_{ab}}{L_{ab}} -$$

$$-F(t)F(u)F(v)F(z)\exp\left(x\frac{q_b}{t^2}\right)\frac{\sin hL_{ab}}{L_{ab}} +$$

$$+F(s)F(t)F(u)\exp[x\left(\frac{q_a}{s^2}+\frac{q_b}{t^2}\right)]\frac{\sin hG_{ab}^{(4)}}{G_{ab}^{(4)}}+$$

$$+F(s)F(t)F(v)\exp[x\left(\frac{q_a}{s^2}+\frac{q_b}{t^2}\right)]\frac{\sin hG_{ab}^{(5)}}{G_{ab}^{(5)}}+$$

$$+F(s)F(t)F(z)\exp[x\left(\frac{q_a}{s^2}+\frac{q_b}{t^2}\right)]\frac{\sin hG_{ab}^{(6)}}{G_{ab}^{(6)}}+$$

$$+F(s)F(u)F(v)\exp\left(x\frac{q_a}{s^2}\right)\frac{\sin hG_{ab}^{(1)}}{G_{ab}^{1}}+$$

$$+F(s)F(u)F(z)\exp\left(x\frac{q_b}{t^2}\right)\frac{\sin hG_{ab}^{(2)}}{G_{ab}^{(2)}}+$$

$$+F(s)F(v)F(z)\exp\left(x\frac{q_a}{s^2}\right)\frac{\sin hG_{ab}^{(3)}}{G_{ab}^{(3)}}+$$

$$+F(t)F(u)F(v)\exp\left(x\frac{q_b}{t^2}\right)\frac{\sin hG_{ab}^{(1)}}{G_{ab}^{(1)}}+$$

$$+F(t)F(u)F(z)\exp\left(x\frac{q_b}{t^2}\right)\frac{\sin hG_{ab}^{(2)}}{G_{ab}^{(2)}}+$$

$$+F(t)F(v)F(z)\exp\left(x\frac{q_b}{t^2})\right)\frac{\sin hG_{ab}^{(3)}}{G_{ab}^{(3)}}+$$

$$+F(u)F(z)F(v)\frac{\sin hL_{ab}}{L_{ab}}-$$

$$-F(s)F(t)\exp[x\left(\frac{q_a}{s^2}+\frac{q_b}{t^2}\right)]-F(s)F(u)\exp\left(x\frac{q_a}{s}\right)\frac{\sin hG_{ab}^{(4)}}{G_{ab}^{(4)}}-$$

$$-F(s)F(v)\exp\left(x\frac{q_a}{s^2}\right)\frac{\sin hG_{ab}^{(5)}}{G_{ab}^{(5)}}-F(s)F(z)\exp\left(x\frac{q_a}{t^2}\right)\frac{\sin hG_{ab}^{(6)}}{G_{ab}^{(6)}}-$$

$$-F(t)F(u)\exp\left(x\frac{q_b}{t^2}\right)\frac{\sin hG_{ab}^{(4)}}{G_{ab}^{(4)}} - F(t)F(v)\exp\left(x\frac{q_b}{t^2}\right)\frac{\sin hG_{ab}^{(5)}}{G_{ab}^{(5)}} -$$

$$F(t)F(z)\exp\left(x\frac{q_b}{t^2}\right)\frac{\sin hG_{ab}^{(6)}}{G_{ab}^{(6)}} - F(u)F(v)\frac{\sin hG_{ab}^{(1)}}{G_{ab}^{(1)}} -$$

$$-F(u)F(z)\frac{\sin hG_{ab}^{(2)}}{G_{ab}^{(2)}} - F(v)F(z)\frac{\sin hG_{ab}^{(3)}}{G_{ab}^{(3)}} +$$

$$F(s)\exp\left(x\frac{q_a}{s^2}\right) + F(t)\exp\left(x\frac{q_b}{t^2}\right) + F(u)\frac{\sin hG_{ab}^{(4)}}{G_{ab}^{(4)}} +$$

$$+F(v)\frac{\sin hG_{ab}^{(5)}}{G_{ab}^{(5)}} + F(z)\frac{\sin hG_{ab}^{(6)}}{G_{ab}^{(6)}} - 1,$$

$$L_{ab} = \sqrt{\left(\frac{q_a}{v^2} + \frac{q_b}{u^2} + 2\frac{\omega_s x}{z^3}\right)^2 + \frac{\omega_s^2}{z^6}(1 + x^2)},$$

$$G_{ab}^{(1)} = \frac{q_a}{v^2} + \frac{q_b}{u^2},$$

$$G_{ab}^{(2)} = \sqrt{\left(\frac{q_b}{u^2} + 2\frac{\omega_s x}{z^3}\right)^2 + \frac{\omega_s^2}{z^6}(1 - x^2)},$$

$$G_{ab}^{(3)} = \sqrt{\left(\frac{q_a}{v^2} + 2\frac{\omega_s x}{z^3}\right)^2 + \frac{\omega_s^2}{z^6}(1 - x^2)},$$

$$G_{ab}^{(4)} = \frac{q_b}{u^2},\ G_{ab}^{(5)} = \frac{q_a}{v^2},\ G_{ab}^{(6)} = \frac{\omega_s}{z^3}\sqrt{3x^2 + 1},\ F(s) = \exp\left(\frac{-\varphi(s)}{kT}\right).$$

The exact form of the pairwise potentials $\varphi_{ab}(R)$ is not known. In the gas approximation they can be calculated by the quantum mechanical methods. The functions thus obtained will hardly be applicable to dense systems in which multi-particle interactions, including participation of a molecule in many $H-$ bonds concurrently, are important. At the same time the structure of the formulas (4) - (6) suggests that the resultant values of $\omega_{ab}(R)$ depend on definite integrals of a function of the type: $r^n \cdot exp(-\varphi_{ab}(R)/kT)$ rather than on the exact potentials $\varphi_{ab}(R)$. Consequently for our purposes the use of simulated potentials φ_{ab} is just sufficient. However, it was of undoubted interest to find the general conditions which the functions $\varphi_{ab}(R)$ should satisfy so that $\omega_{ab}(R)$ may qualitatively agree with the properties of $1 - 1$ aqueous electrolytes found

in experiments. Hence, the potentials $\varphi_{ab}(R)$ were chosen as follows: (a) the Lennard-Jones potentials from the data of [8] (Fig. 1); and (b) the essentially non-Lennard-Jones potentials, deeper and wider (Fig. 2), whose shape could be predicted from purely theoretical conjectures [9], including those which take into account the partial charge transfer occurring in an ion-molecule interaction [10]. In the calculations the pairwise potentials were tabulated and in the computation process they were interpolated by cubic splines[11]. Calculation of integrals by this method under the Gaussian scheme chosen gives an accuracy of the oder of 10   (1%).

All calculations, except for some special cases, were made using the following parameter values: $Z_a = 1, Z_b = -1, P_s = 2D, n_s^* = 0, 5, T = 298.16°K$.The numbers of the $\omega_{ab}(R)$ curves refer of the numbers of the $\varphi_{ab}(R)/kT$ curves shown in respective figures and used in the present calculations; the first number refers to the potential $\varphi_{as}(R)$, the second number refers to the potential $\varphi_{bs}(R)$, the third to $\varphi_{ss}(R)$.

APPROXIMATION OF THE 3-RD VIRIAL CO-EFFICIENT

The $\omega_{as}(R)$ versus $\varphi_{as}(R)$ relatioship. Fig. 3 illustrates typical calculated results. It is seen that for relatively weak ion-solvent molecule interactions (Potential 4 and 5) the curve $\omega_{ab}(R)$ has a deep minimum indicating the existence of contact ion pairs for the values of σ_{ab} determined by the form of the potential $\varphi_{ab}(R)$ (Fig. 1,Curve 6.) With the increasing interaction between ions and the solvent simulated by an arbitrary set of potentials selected from those shown in Fig. 1, the probability of formation of contact ion pairs decreases (the absolute minimum depth decreases), while in the range of large R the curve suffers a bend which, as the interaction increases, transforms into the second, less deep, minimum. It is located at $R < \sigma_{as} + \sigma_{bs}$, that is, the probability of formation of solvent-shared ion pairs of nonlinear structure is higher than that of linear structure(with the ⓐⓢⓑ arrangement).

Fig. 4 shows the results obtained under the assumption that the ion-solvent interaction is strong. Comparison of the curves calculated for the potentials I-I and II-II shows that an increase of interaction reduces the deviation of the solvent molecule from the line of ion centers (the minimum shifts towards higher R) and at $R = \sigma_{ab}$ the minimum vanishes; in the range where $R \approx \sigma_{ab}$ $\omega_{ab}(R)$

becomes positive manifesting the instability of the contact ion pairs. In case only one of the ions interacts strongly with the solvent, both minima remain, but unlike the case of weak interaction, the second minimum is deeper than the first one, i.e. the relative concentration of shared pairs is greater than that of the contacting pair.

The concentration of contact ion pairs in typical I-I electrolytes solutions, say LiCl solution, is negligibly small at low concentrations. It was therefore of special interest to find out whether this result could be obtained by modifying the potentials 4 and 5, Fig. 1, within reasonable limits. Such modification is plotted in Fig. 5 and the corresponding functions in Fig. 6. From these results as well as from their comparison with those mentioned above it follows that in a real aqueous LiCl solution the pairwise interactions of ions with the solvent should be much stronger than those predicted by the Lennard-Jones potentials. Experiment confirms this conclusion, since chlorine ions are known to form H—bonds with water molecules [1] and since partial charge transfer occurs in the interaction between lithium ion and water [10].

The $\omega_{ab}(R)$ versus P_s relationship. This relationship is shown in Fig. 7. It follows that the increase of P_s is generally equivalent to the increase of the ion-solvent interaction represented by functions $\varphi_{as}(R)$.

The $\omega_{ab}(R)$ versus n_s^* relationship. For real water $n_s^* = 0.25$. It is physically obvious that an increased number of solvent particles in a unit volume should enhance the probability of the ⓐⓢ configurations and reduce that of the ⓐⓑ configurations. Accordingly, probability of the ⓐⓢⓑ type configurations should increase, too. Fig. 8 shows that this is precisely the case, i.e. the increase of N_s^* is indeed equivalent to the increase of P_s.

The $\omega_{aa}(R)$ potentials. The model potentials shown in Fig. 1 and Fig. 9 were used in the calculations which sufficiently clarified the situation. From Fig. 10 it is seen that, as in the case of oppositely charged ions, stable shared ion pairs are formed under sufficiently strong ion-solvent interaction. However, there is a remarkable difference, too: the minimum of $\omega_{ab}(R)$ is located exactly at $R = 2\sigma_{as}$ which corresponds to a strictly linear arrangement of the three particles a s a. Physically, it is evident that the reason is the mutual repulsion of like charges. As regards the possibility of the existence of compact configurations comprising ions of like charges it must be noted that they have been discovered experimentally [12] and are formed precisely due to specific ion-water interaction.

8

The variations in P_s and N_s^* at fixed potentials $\varphi_{as}(R)$ affect $\omega_{aa}(R)$ in the same manner (Figs 11 and 12) as they do the functions $\omega_{ab}(R)$ (Figs 7 and 8).

The effect of temperature both on $\omega_{ab}(R)$ and $\omega_{aa}(R)$ investigated in the range from 273 to 283 K was insignificant and below 0.5%. This is consistent with the results of [2], according to which the temperature variations in these functions of the same small order are required to calculate the heats of dilution of strong electrolytes from empirical MFP.

APPROXIMATION OF THE 4-th VIRIAL CO-EFFICIENT

In this approximation the contribution of the elementary diagram is neglected, which corresponds to the hyperchain approximation in the theory of simple systems with short-range potentials $\varphi_{ab}(R)$ [13].

The $\omega_{ab}(R)$ versus $\varphi_{ab}(R)$ relationship. Allowance for the solvent "structure" elements in terms of $\varphi_{ss}(R)$ considerably complicated the overall picture. Fig. 13 shows the results obtained at a fixed potential $\varphi_{ss}(R)$. Our attention is drawn to the absence of minimum at $R = \sigma_{ab}$ even for weak ion-solvent interactions (Curves 1 and 3), observed in the 3rd virial coefficient approximation at R values up to rather strong ion-solvent interactions (cf. Figs 3, 4 and 6). In other words, the direct allowance for the intermolecular interactions is essential for a correct (even qualitative) description of ion distribution nature in the ion-dipole systems. The authors of [14] were the first to emphasize the importance of taking into account the 4-th virial coefficient in this respect. The position of the first minimum between $\sigma_{ab} < R < \sigma_{ab} + \sigma_{bs}$ suggests that it

relates to configurations of the ⒜ⓢⓑ type, or more likely, to ⒜ⓢⓑ type, since only intermolecular interaction can prevent formation of contacting ion pairs. The configurations of the second type are indeed responsible for the nontrivial shift of the first minimum in R, depending on the potentials $\varphi_{as}(R)$ (cf. Fig. 13a). This idea is supported by Fig. 14 as well, which shows that the minimum shifts slightly towards larger R with the increasing potential $\varphi_{ss}(R)$ depth (Fig. 15), which is equivalent to transformation of the configurations of

the form ⒜ⓢⓑ to configurations of the form ⒜ⓢⓑ .A further increase

in the solvent-solvent interaction gives rise to positive $\omega_{ab}(R)$ in the vicinity of the first minimum (Fig. 15), i.e. the foregoing configurations become unstable.

The second minimum in Fig. 13 corresponds to inter-ion distances $R = \sigma_{as} + \sigma_{ss} + \sigma_{bs}$ (Curve I) under a weak interaction. The corresponding linear configuration is (a)(s)(s)(b) . With the increasing interaction between ions and solvent, the minimum shifts towards smaller R indicating that the configurations of the type (a)(s)(s)(b) predominate, and on further enhancement (Curve 4) the minimum degenerates into a horizontal portion signifying the existence of a set of approximately equiprobable configurations of this type. The decline of Curve 4 towards the first minimum begins at R larger than for the configuration (a)(s)(b) .

The $\omega_{ab}(R)$ versus P_s relationship is shown in Fig. 16. On the whole, an increase of P_s affects the first minimum depth in the same direction as an increase of the ion-solvent interaction while on the second minimum depth, as an increased solvent-solvent interaction.

The $\omega_{ab}(R)$ versus n_s^* relationship. On the whole, an increase of n_s^* affects $?_{ab}(R)$ in the same direction as an increase in the molecule-molecule interaction. In particular, at low solvent density (the "gas" approximation) the curve $\omega_{ab}(R)$ has only one minimum corresponding to the formation of contacting solvated ion pairs of the type (a)(s)(s)(b). As n_s^* increases, its ordinate increases too, shifting towards positive values, and simultaneously the second minimum begins to appear corresponding to the formation of the shared ion pairs of the type (a)(s)(s)(b) (Fig. 17). It is importat, however, that for a particular set of potentials, by varying n_s^* it is not possible to convert, the curves given in Fig. 17a into curves such as Curve 4 of Fig. 17b whose maximum lies in the negative region of $\omega_{ab}(R)$. The necessary and sufficient condition for such a conversion is the enhanced molecule-molecule interaction. Water density is 55 moles per liter, that is, $n_s^* = 0.25$. Accordingly, Curve 4 (Fig. 17b) provides a qualitative description of a situation frequently occurring in aqueous solutions, namely, when hydrated and shared ion pairs coexist in equilibrium easily passing into each other [15]. Calculations show that this situation is more accurately described by the Guggenheim-McGlachan [16] potentials than by the

Lennard-Jones potentials. This agrees well with the results of [17] in which the radial distribution functions of liquid argon calculated under the hyperchain approximation were found to agree with the experiments if the potentials [16] were used instead of the Lennard-Jones potentials.

The $\omega_{aa}(R)$ potentials. The main results shown in Fig. 18 suggest that, firstly, in the 4th virial coefficient approximation the minimum corresponds to the formation of ion pairs in which the ions are separated by two solvent molecules rather than by one as in the 3rd virial coefficient approximation (cf. Fig. 10); and secondly, that the deepening of both potential $\varphi_{as}(R)$ and potential $\varphi_{ss}(R)$ increases the probability of the occurrence of the same configuration (a)(s)(s)(b) which constitutes the principal difference from the interaction between ions of unlike charge.

EFFECT OF THE ELEMENTARY DIAGRAM OF THE FOURTH VIRIAL COEFFICIENT

The contribution of diagram for typical sets of potentials is shown in Fig. 19. It is seen that the contribution is considerable even at relatively weak potentials (Curve 1) and it increases especially on transition to the non-Lennard-Jones potentials (Curve 3) of the type shown in Fig. 20.

In Fig. 21 the results calculated for all the three approximations are compared. Here three points deserve our attention. First, an account of the elementary diagram for not very deep potentials $\varphi_{as}(R)$ provides for the coexistence of configurations (a)(s)(b) and (a)(s)(s)(b) , Fig. 21a. Second, for deeper potentials $\varphi_{as}(R)$ the probabilities of the occurrence of these configurations become closer, Fig. 21b. Third, calculations show that the evaluation of the MFP and the physical assumptions deduced for the interparticle interactions made in the hyperchain approximation, i.e. without an account of the elementary diagram, and based solely on the agreement between the theoretical and experimental thermodynamical properties of electrolytic solutions [5, 18], must be used very cautiously. The reason is that the elementary diagram does make a considerable quantitative contribution into the MFP, and the calculations have been shown in [2] to be very sensitive to the MFP.
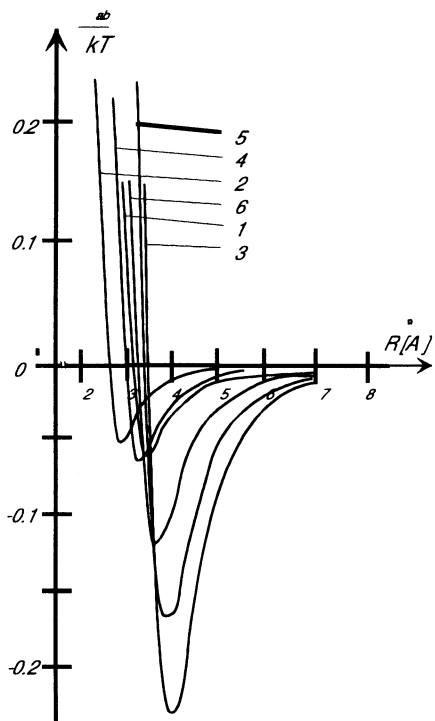
Figure 1: Lennard-Jones potentials according to [8]:1 — $H_2O - H_2O$, 2 — $Li^+ - Li^+$, 3 — $Cl^- - Cl^-$, 4 — $Li^+ - H_2O$, 5 — $Cl^- - H_2O$, 6 — $Li^+ - Cl^-$
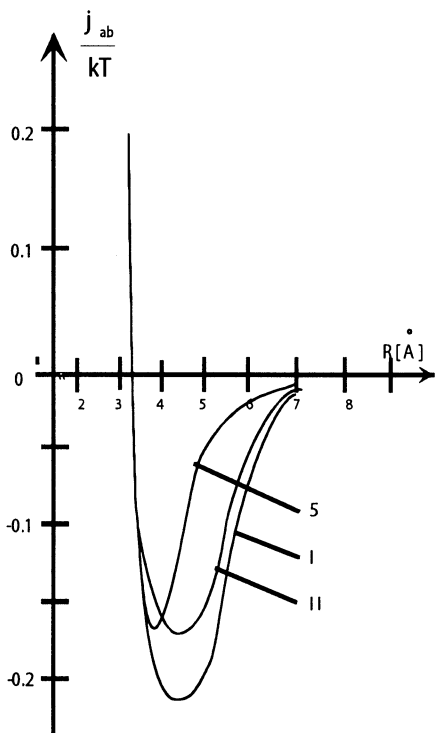
Figure 2: Model potentials. Curve 5 from Fig. 1 is shown for the purpose of comparison
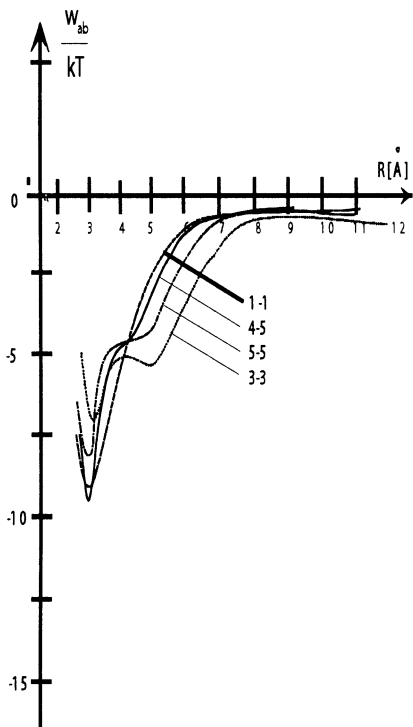
Figure 3: $\omega_{(ab)}(R)$ functions computed with potentials $\varphi_{(ab)}(r)$ shown in Fig. 1. The 3–rd virial coefficient approximation.
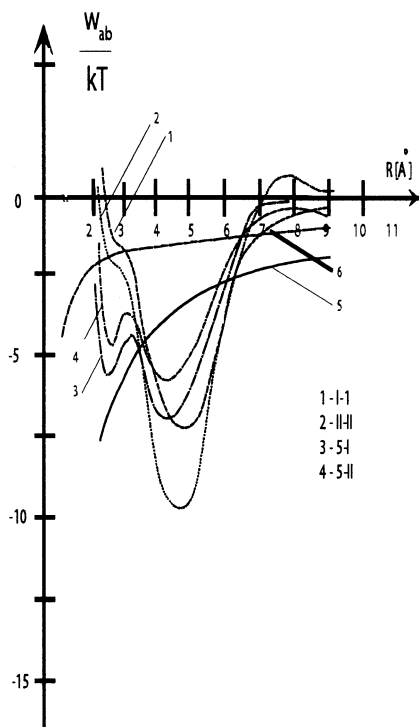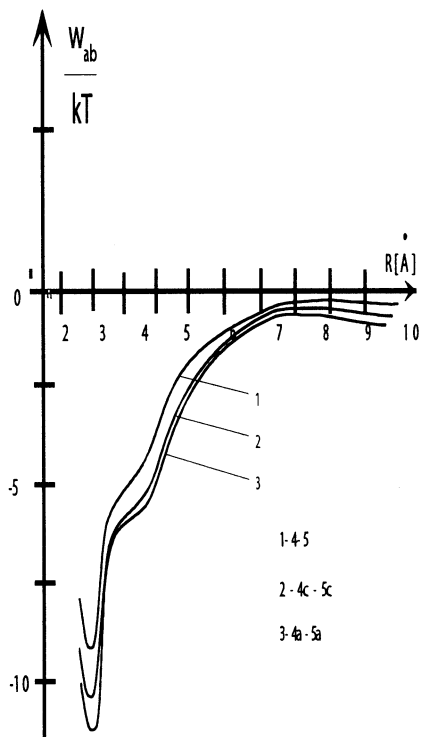
Figure 4: $\omega_{(ab)}(R)$ functions computed for strong interaction of solvent molecule with both ions (curves 1 and 2) and with one ion (curves 3 and 4); Coulomb potentials, $Z_a Z_b e^2/\varepsilon r$: $5 - \varepsilon = \varepsilon_0$, $6 - \varepsilon = 74.45$. The 3rd virial coefficient approximation.
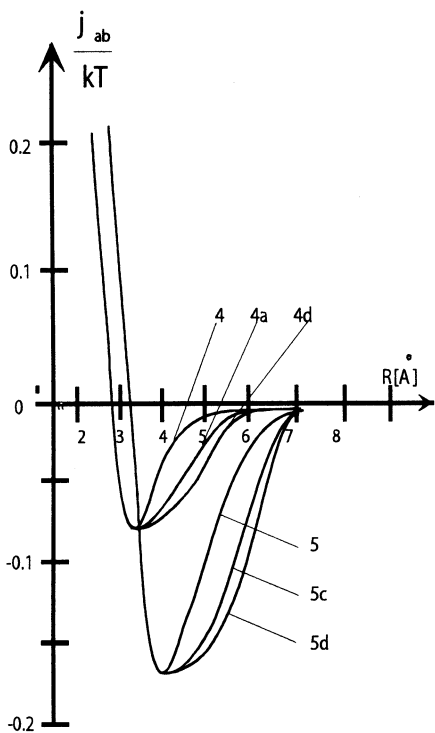
Figure 5: Modified Lennard–Jones potentials 4 and 5 of Fig. 1.

Figure 6: $\omega_{ab}(R)$ computed with the potentials $\varphi_{as}(R)$ shown in Fig. 5. The 3rd virial coefficient approximation
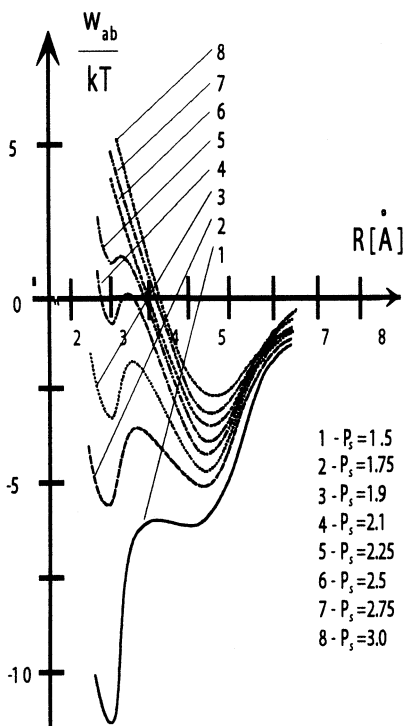
Figure 7: The effect of P_s on the probability of formation contact and solvent–shared ion paris. The $\varphi_{as}(R)$ potential is the F_2 potential shown in Fig. 15. The 3rd virial coefficient approximation.
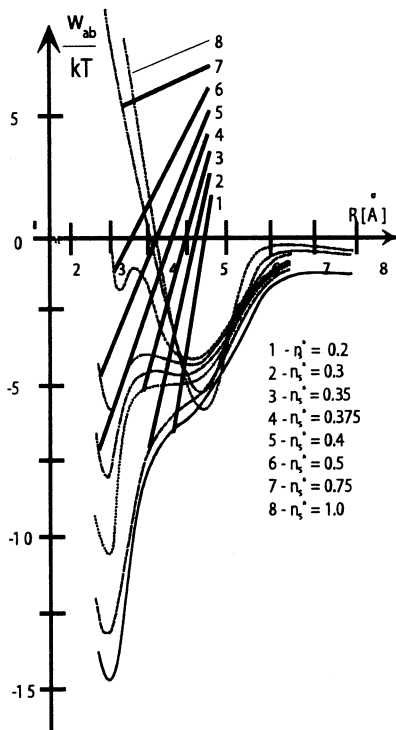
Figure 8: The effect of solvent number density on the probability of formation of contact and solvent–shared ion pairs. The $\varphi_{as}(R)$ potential is taken as the F_2 potential shown in Fig. 15. The 3rd virial coefficient approximation.
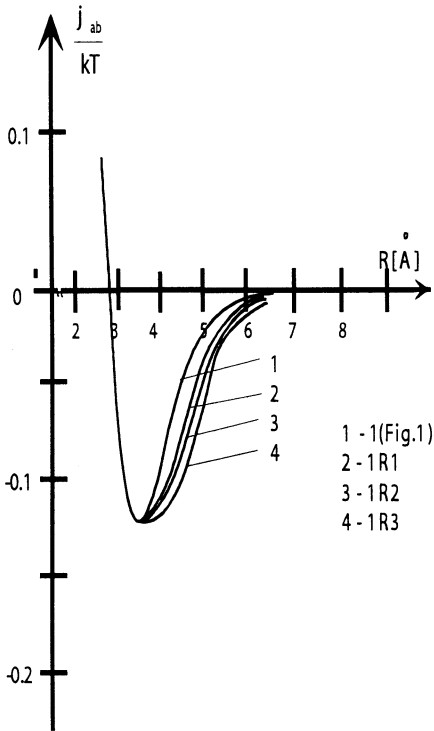
Figure 9: Another set model potentials.
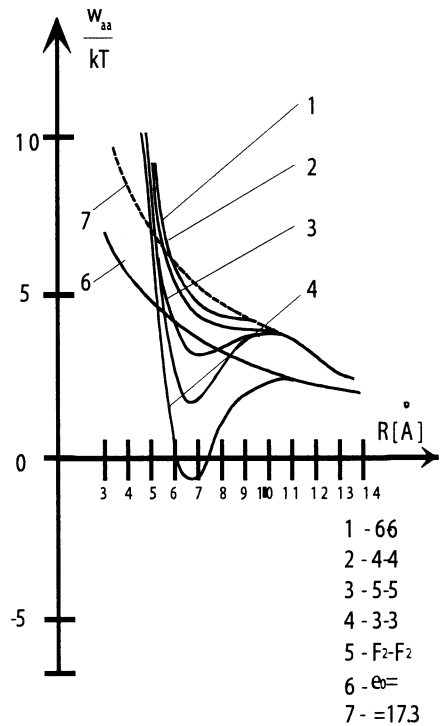
Figure 10: $\omega_{aa}(R)$ functions computed with the potentials $\varphi_{as}(R)$ shown in Fig. 1 and Fig. 15. The 3rd virial coefficient approximation.
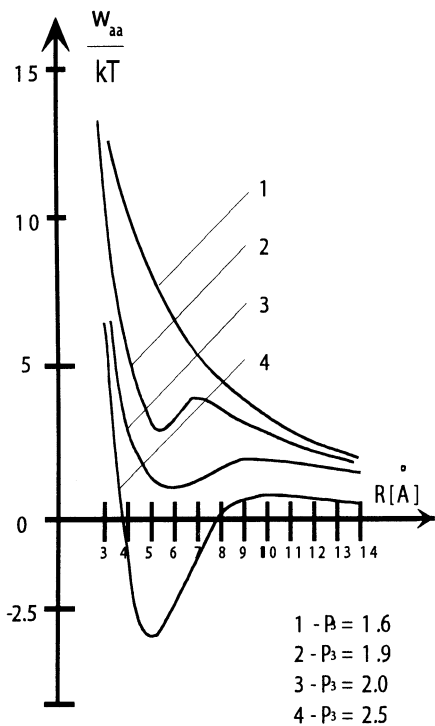
Figure 11: The effect of P_s on $\omega_{aa}(R)$ functions. The $\varphi_{as}(R)$ potential is taken as the IR potential shown in Fig. 9. The 3rd vitial coefficient approximation.
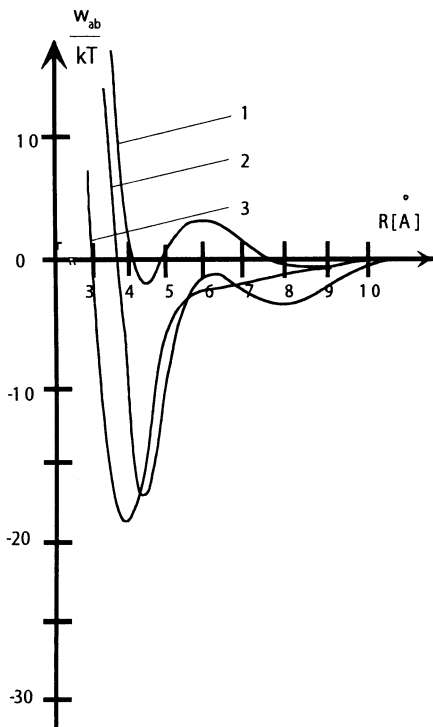
Figure 12: The effect of solvent number density on $\omega_{as}(R)$ functions. The $\varphi_{as}(R)$ potential is taken as the TRI potential shown in Fig. 9. The 3rd virial coefficient approximation.

17

Figure 13: $\omega_{ab}(R)$ functions calculated with fixed $\varphi_{ss}(R)$ potentials, Fig. 1, curve I, and various $\varphi_{as}(R)$ potentials: I— 6–6–I, 2— 5–5–I, 3— 4d–4d–I.
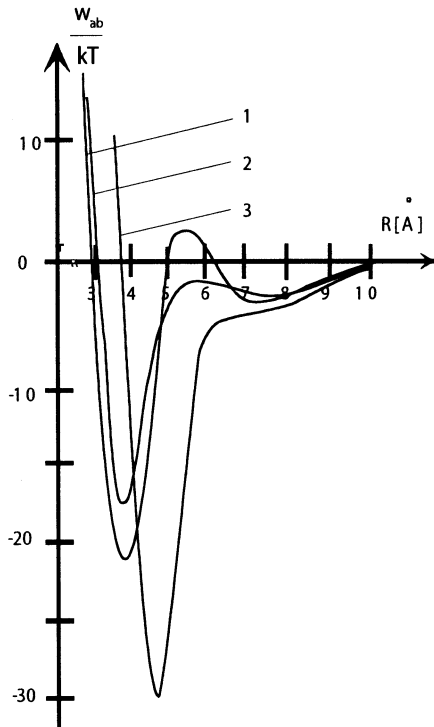
Figure 14: $\omega_{ab}(R)$ functions calculated with fixed $\varphi_{ss}(R)$ potentials, Fig. 1, curve I, and various $\varphi_{as}(R)$ potentials: I— 3–5–1, 2— I–4–I, 3—I–3–I.
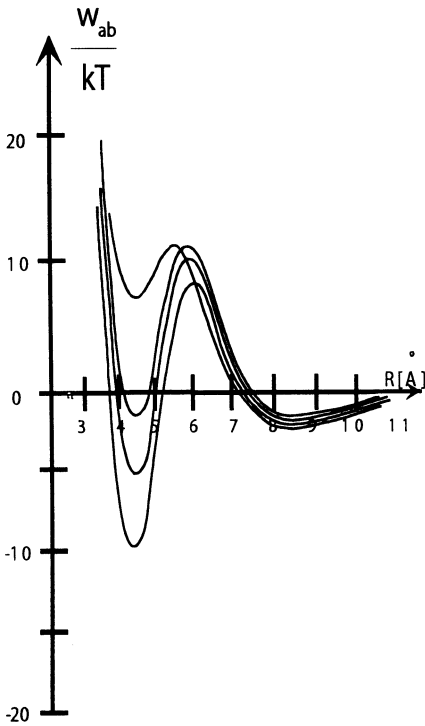
18

Figure 15: $\omega_{ab}(R)$ functions calculated with fixed $\varphi_{as}(R)$ and $\varphi_{bs}(R)$ potentials and various $\varphi_{ss}(R)$ potentials: $\varphi_{as}(R)$— Fig. 1, curve 4, $\varphi_{bs}(R)$ — Fig. 1, curve 5; $\varphi_{ss}(R)$: I—F_i, Fig. 15, 2— F_3, Fig. 15, 3 — F_5, Fig. 15, 4— IR3, Fig. 9.
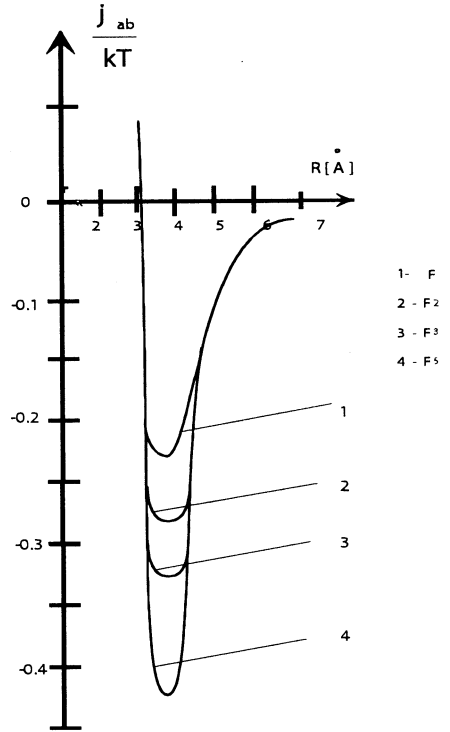
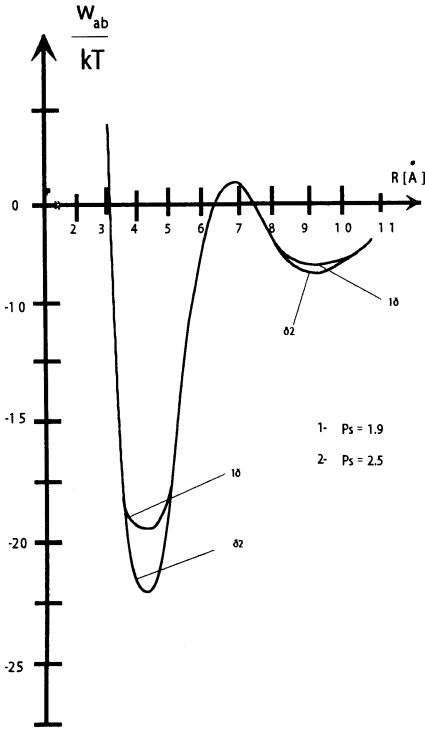Figure 16: Model potentials differing one from another only by their depths.

Figure 17: The effect of P_s on $\omega_{ab}(R)$ functions calculated under condition that $\varphi_{as}(R) = \varphi_{ba}(R) = \varphi_{ss}(R)$ =potential 3 of Fig. I.
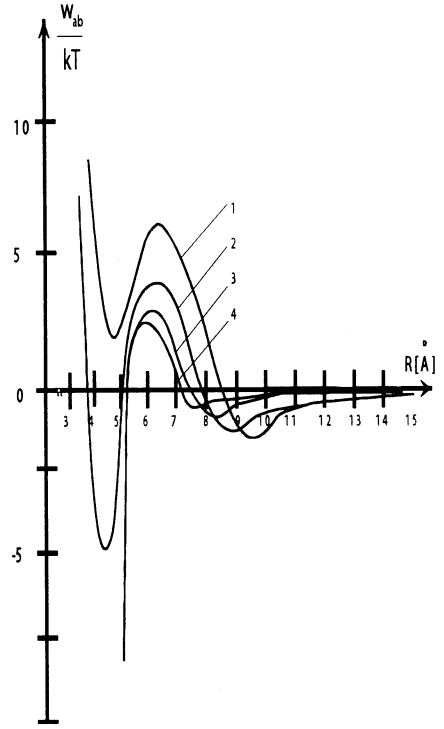
Figure 18: The effect of n_s^* on $\omega_{ab}(R)$ functions in case of strong molecule–molecule interactions; set of potentials 4–5–F_2 : I — $n_s^* = 0.5$, $2 - n_s^* = 0.4$, 3— $n_s^* = 0.3$, $4 - n_s^* = 0.25$, $5 - n_s^* = 0.2$, $6 - n_s^* = 0.1$.
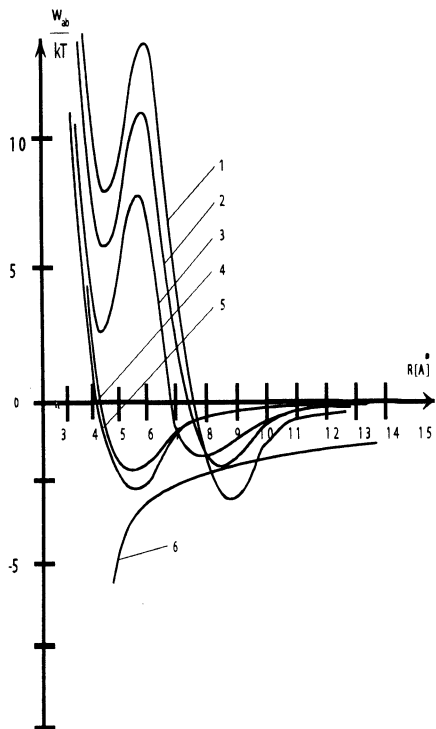
Figure 19: The effect of n_s^* on $\omega_{ab}(R)$ functions in case of weak molecule-molecule interactions; set of potentials 4–5–IR2: I— $n_s^* = 0.5$, 2— $n_s^* = 0.4$, 3— $n_s^* = 0.3$, 4— $n_s^* = 0.2$.
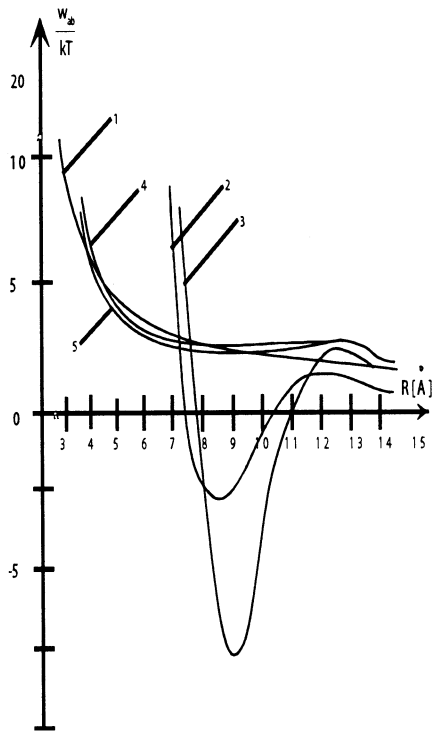
Figure 20: $\omega_{aa}(R)$ functions calculated with potentials shown in Fig. 1. I — Coulomb law, $\varepsilon = 74.45$; 2—5— $\omega_{aa}(R)$ functions for sets of model $\varphi_{aa}(R)$ potentials: 2— 5–5–I, 3— 5–5–3, 4— 4–4–I, 5— 4–4–3. The 4th virial coefficient approximation.
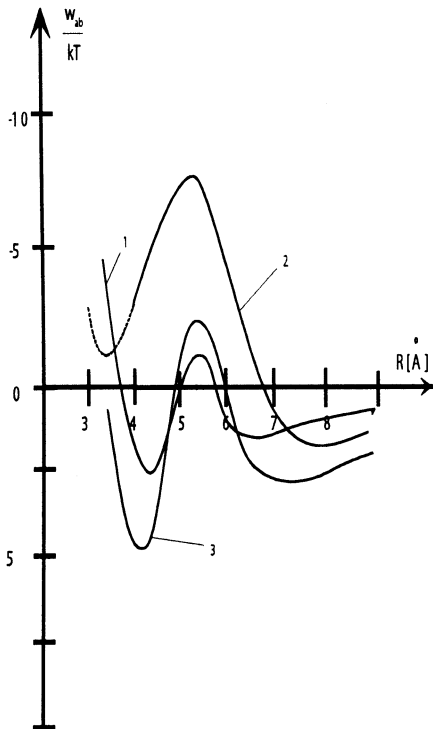
Figure 21: The contribution of the elementary to $\omega_{ab}(R)$ functions. Set of $\varphi_{as}(R)$ potentials (Fig. 1 and Fig. 20): I — 4–5–5, 2— 3–3–3, 3— 4–5–F_s.
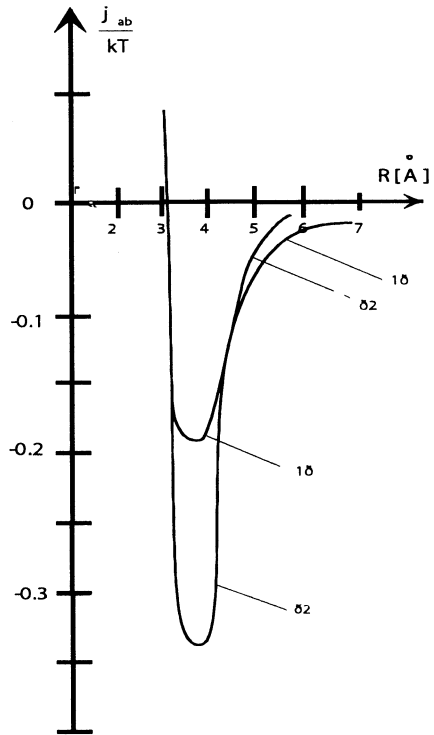
Figure 22: Tangibly not a Lennard–Jones potential, F_3, used for computing the elementary diagram: I — potential F of Fig. 15, 2— F_s.
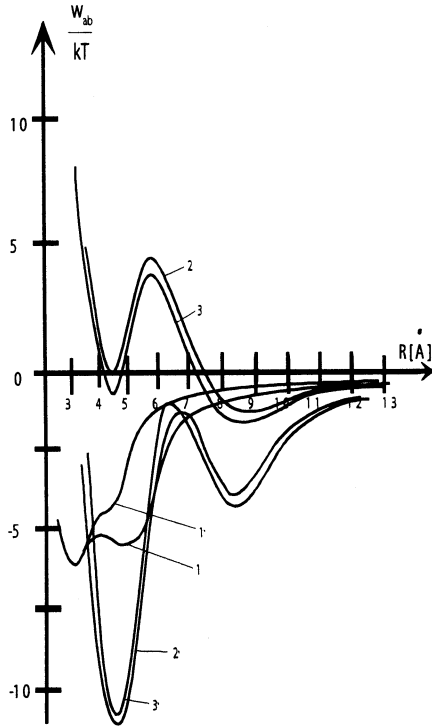
Figure 23: Comparison of $\omega_{ab}(R)$ functions computed in various approximations: a) set of $\varphi_{ab}(R)$ potentials: 4–4–5; I — the 3rd virial coefficient approximation, 2 — the HNC approximation, 3— the HNC approximation plus the contribution of elementary diagram. b) set of $\varphi_{ab}(R)$ potentials: 3–3–5, I — the 3rd virial coefficient approximation, 2 — the HNC approximation, 3— the HNC approximation plus the contribution of the elementary diagram.

CONCLUSIONS

The virial series used for the evaluation of the inter-ion MFP cannot probably be restricted to the fourth virial coefficient. This doubt arises due to the strong difference between the $\omega_{ab}(R)$ functions calculated in the 3rd and 4th virial coefficient approximation as well as due to the considerable difference in the sensitivity of $\omega_{ab}(R)$ to P_s variations in these approximations. Nevertheless, the calculation results do provide a qualitatively authentic physical picture which is experimentally observed in strong electrolyte solutions. In particular, an increased interaction between ion and molecule enhances the probability of formation of ion pairs in which the ions are separated by one solvent molecule, and an increased molecule-molecule interaction simulating the growth of solvent «structuredness» enhances the probability of the formation of ion pairs in which the ions are separated by two solvent molecules. Further, special calculations made for smaller ions have shown that a stronger ion-solvent interaction is required to form the shared rather than contact ion pairs. Finally, the MFP have a regular asymptote corresponding to the Coulomb potential with $\varepsilon = 74.45$. However, such an asymptotic behaviour is observed for unlike charged ions in the third virial coefficient approximation (Fig. 4) and for ions of like charge only in the 4th virial coefficient approximation (Fig. 18), whereas in the third virial coefficient the asymptote, while still remaining Coulomb, has $\varepsilon = 17.3$ (Fig. 10).

Hence it may be noted that the treatment of inter-ion MFP in an ion-dipole system with the Lennard-Jones potentials by the Monte-Carlo method [19 has yielded functions similar to the Curve 5-5 in Fig. 3 (with a deep minimum corresponding to the formation of contact ion pairs and a feeble likeness of a second minimum at R values corresponding to the formation of shared ion pairs). This simple result is probably due to the specific features of the Monte-Carlo method. Indeed, the MFP of methane-methane interaction in water calculated by this method resulted in a curve having one minimum at the contact region [20], whereas the theoretical treatment resulted in a curve with several extrema [21].

The last fact to be noted here is the instability of the second minimum relative to weak $\varphi_{as}(R)$ variations (Fig. 13) and small density variations (cf. Fig. 8). The situation resembles phase transformation and can indeed be due to jump-like variation of the nearest neighbour distribution, in our case - to a change from one ion pair type to another. A natural way to clarify this and some other still unclarified points is to calculate the contribution of the

next virial coefficients and the MFP of the molecule-molecule and ion-molecule interactions.

References

[1] H.L. Friedman, C.V. Krishnan. Thermodynamics of Ion Hydration. In "Water. A Comprehensive Treaties", ed. by F.Francks, vol.3, Plenum Press, N.Y.G., 1973.

[2] Yu. M. Kessler, V. D. Grouba, V. A. Kiryanov, V.P. Yemelin. Adequacy of Parameters in Statistical-Mechanical Calculations of the Properties of Strong Electrolyte Solutions. J.Sol.Chem. 1977, v.6,No.4, 231-250.

[3] M. Born. Volumen und Hydratationswärme der Ionen. Z. fur Physik, 1920,v.1,No.1, 45-48.

[4] P. Debye, E. Huckel. Zur Theorie der Elektrolyte. Phys. Fceite. 1923.v.24,No.9, 185-206.

[5] P. S. Ramanathan, C.V.Krishnan, H. L. Friedman. Models Having the Thermodynamic Properties of Aqueous Solutions of Tetraalkylammonium Halides. J.Sol.Chem. 1972, v.1,No.3,237-262.

[6] I. R. Yukhnovsky. Some Aspects of Current Theories of Equilibrium Systems of Charged Particles. Ukranian Phys. J. 1969, v.14,No.5, 705-719.

[7] I. R. Yukhnovsky, M.P.Golovko, V.S.Vysochansky. Investigation of Pair Distribution Functions for Ion-Dipole Mixtures Expressed as the Exponent of Average Force Potential. Ukrainian Phys. J.1977,v.22,No.8,1330-1339.

[8] K. Heinzinger, P. C. Vogel. A Molecular Dynamics Study of Aqeuous Solutions. Zaeits.Naturforsch.1974,v.29a,No.8t1164–1171.

[9] M. I. Shakhparonov. Introduction to Contemporary Theory of Solutions. "Nauka", M.,1976.

[10] A. I. Mishustin,Y. M. Kessler. Ion-Solvent Interaction in Non-aqueous Solutions. Spin-Lattice Relaxation. J.Sol.Chem. 1975,v.4,No.9,779-782.

[11] C. H. Reinsch. Smoothing by Spline Functions. Numer.Math. 1967,b.10,h.3,177-183.

[12] Y. M. Kessler. Doct.Thesis. Institute of Electrochemistry of Academy of Sciences of the USSR,M.,I969, 327p.

[13] G. Stall. Cluster Expansions for Classical Systems in Equilibrium. In "The Equilibrium Theory of Classical Fluids".

[14] I. R. Yukhnovsky, V. S. Vysochansky, M. F. Golovko. Pair Correlation Functions for Ion-Dipole Mixtures in the Fourth Virial Coefficient Approximation. Ukrainian Phys. J. 1975,v.20,No.5,817-828.

[15] M. Eigen. Determination of General and Specific Ionic Interactions in Solutions. Disc. Farad. Soc. 1957, v(n)24, 24-36.

[16] E. A. Guggenheim, M. L. McGlashan. Interaction between Argon Atoms. Proc.Roy.Soc. (L)1960, V.A255,No.283,456-476.

[17] A. A. Khan. Radial Distribution Function of Fluid Argon. Phys.Rev.1964,r.134, No.2AfA367-384.

[18] J. C. Raeaiah, H. L. Friedman. Integral Equation Methods in the Computation of Equilibrium of Ionic Solutions. J. Chem.Phys. 1968,v.48,No.6,2742-2752.

[19] I. R. McDonald, J. C. Raeaiah. Monte Carlo Simulation of the Average Force between Two Ions in a Stockmayer Solvent. Chem. Phys. Left. 1975,v.34,No.2,382-386.

[20] V. G. Dashevsky, G. N. Sarkisov. The Solvation and Hydrophobic Interaction of Non-Polar Molecules in Water in Approximation of Interatomic Potentials: The Monte Carlo Method. Mol. Phys. 1974,v.27,No.5, 1271-1290.

[21] D. Chandler. Theory of the Hydrophobic Effect, J.Chem. Phys. 1977, v.67, No.8, 3683-3704.

Айрян Э. А., Груба В. Д., Сидоренко С. Н.
Е11-2002-260

Роль взаимодействий ион–молекула и молекула–молекула
в формировании потенциала средней силы
взаимодействия двух ионов

В рамках классической ионно-дипольной модели растворов электролитов исследовано влияние ион-молекулярных и межмолекулярных взаимодействий на формирование межионных потенциалов средней силы. Показано, что последние на больших расстояниях обладают кулоновской асимптотикой, а в области средних расстояний имеют форму, описывающую образование и распад сольватно-разделенных ионных пар. Результаты численных расчетов дают качественно правдоподобную картину, которая экспериментально наблюдается в растворах сильных электролитов. В частности, сильное ион-молекулярное взаимодействие способствует образованию таких ионных пар, в которых ионы разделены одной молекулой растворителя.

Ayrjan E. A., Grouba V. D., Sidorenko S. N.
Е11-2002-260

The Role of the Ion–Molecule and Molecule–Molecule Interactions
in the Formation of the Two-Ion Average Force
Interaction Potential

The effect of the ion-molecular and intermolecular interactions on the formation of inter-ion average force potentials is investigated within the framework of a classical ion-dipole model of electrolyte solutions. These potentials are shown to possess the Coulomb asymptotic at large distances while in the region of mean distances they reveal creation and disintegration of solvent-shared ion pairs. The calculation results provide a qualitatively authentic physical picture which is experimentally observed in strong electrolytes solutions. In particular, an increased interaction between ion and molecule enhances formation of ion pairs in which the ions are separated by one solvent molecule.

Макет *Т. Е. Попеко*